Author/s:
Harley, WS;Kolesnik, K;Heath, DE;Collins, DJ

Title:
Enhanced acoustic streaming effects via sharp-edged 3D microstructures

Date:
2024-03-21

Citation:
Harley, W. S., Kolesnik, K., Heath, D. E. & Collins, D. J. (2024). Enhanced acoustic streaming effects via sharp-edged 3D microstructures. Lab on a Chip: miniaturisation for chemistry, physics, biology, materials science and bioengineering, 24 (6), pp.1626-1635. https://doi.org/10.1039/d3lc00742a.

Persistent Link:
https://hdl.handle.net/11343/343936

Enhanced acoustic streaming effects via sharp-edged 3D microstructures

William S. Harley[1,2,3], Kirill Kolesnik[1,3], Daniel E. Heath[1,3], David J. Collins[1,3]
[1]Department of Biomedical Engineering, University of Melbourne, Melbourne, VIC 3010, Australia
[2]Micro Nano Research Facility, RMIT University, Melbourne, Victoria 3000, Australia
[3]The Graeme Clark Institute, The University of Melbourne, Parkville, VIC, 3010, Australia

Corresponding author: david.collins@unimelb.edu.au

Abstract

Acoustofluidic micromanipulation is an important tool for biomedical research, where acoustic forces offer the ability to manipulate fluids, cells, and particles in a rapid, biocompatible, and contact-free manner. Of particular interest is the investigation of acoustically driven sharp edges, where high tip velocity magnitudes and strong acoustic potential gradients drive rapid motion. Whereas prior devices utilizing 2D sharp edges have demonstrated promise for micromanipulation activities, taking advantage of 3D structures has the potential to increase their performance and the range of manipulation activities. In this work, we investigate high-magnitude acoustic streaming fields in the vicinity of sharp-edged, sub-wavelength 3D microstructures. We numerically model and experimentally demonstrate this in fabricating parametrically configured 3D microstructures whose tip-angle and geometry influence acoustic streaming velocities and the complexity of streaming vortices, finding that the simulated and realized velocities and streaming patterns are both tunable and a function of microstructure shape. These sharp-edge interfaces hold promise for biomedical studies benefiting from precise and targeted micromanipulation.

Keywords: Acoustic micromanipulation, Sharp-edge microstructures, Acoustic streaming, Two-photon lithography

1. Introduction

Microfluidic systems have been utilized in a range of applications, including for drug discovery, diagnostics, and bioreactions[1-3], where small sample volumes, high sensitivity, rapid reaction kinetics, and integrative capabilities make microfluidics an ideal tool for controlling microscale environments[4-6]. An important characteristic of these systems is the ability to effectively manipulate fluids and micro-objects. Various physical effects have been utilized for micromanipulation beyond hydrodynamic forces, including optical tweezers[7, 8], magnetophoresis[9, 10], dielectrophoresis[11, 12], and acoustophoresis[13, 14]. Optical, magnetic, and electric approaches, however, often require high power intensities, have poor spatial selectivity, or have negative effects on biocompatibility[15-17]. Acoustic approaches,

conversely, can perform contactless and label-free manipulation while maintaining long-term cell viability[18-20]. Acoustic fields have accordingly demonstrated good biocompatibility at the applied powers necessary for rapid manipulation effects across a wide range of operating frequencies (kilohertz to gigahertz)[21, 22]. Whereas much of acoustofluidic work has exploited simple periodic patterns using standing waves[23, 24], recent efforts have demonstrated that the interaction between acoustic field and complex structures has the potential to further enhance the spatial selectivity and complexity of acoustic manipulation [25-27].

Acoustofluidic effects around oscillating sharp edges, for example, have been used to induce fluid mixing, pumping, and particle manipulation[28-30]. Sharp-edge microstructures are typically fabricated as a component of a microfluidic channel wall, protruding into the fluid domain and presenting a single line-shaped edge at the apex. Alternatively, robotic actuated vibrating needles have been explored as well[31]. When channel-bonded 2D structures oscillate in response to acoustic excitation, the sharp-edge generates a pair of counter-rotating vortices (double-ring recirculating flows) around the apex[32-34]. Sharp-edged structures can produce streaming velocities that are several orders of magnitude higher than those of Rayleigh streaming at similar vibrational amplitudes[35, 36]. These acoustic streaming effects accordingly facilitate on-demand mass transport of fluids and particles[37-40]. Huang et al., for instance, demonstrated the potential of acoustically driven sharp-edge structures for rapid and homogenous mixing in microfluidic devices [41]. Pavlic et al. also utilized oscillating channel boundary sharp-edges for the creation of a programmable acoustofluidic pump[42]. Wang et al. further highlighted how high shear forces in such devices can be used to perform cell lysis[43].

Together, these acoustic-structure approaches demonstrate the ability to effect micromanipulation beyond the formation of periodic, wavelength-scale streaming vortices that are typical of standing wave acoustic devices[44-46]. A common outcome of this work is that sharper edge tips result in higher streaming velocities and an increased spatial extent of the induced streaming, producing amplified acoustic force gradients by decreasing the angle of a sharp edge's apex[47-49]. Whilst a variety of microstructures have been used to generate amplified microstreaming effects via sharp-edge geometries, they have been constrained in terms of their versatility, primarily being limited to boundary-driven arrangements on channel sidewalls, generating vortical flow across a channel cross-section. The complexity of these structures is also limited, where sharp-edge interfaces generally utilize oscillating 2-dimensional straight edges in etched/molded channels that generate streaming vortices that are orthogonal to the sharp edge. These limitations ultimately arise from the dimensionality of the structures and fabrication methods utilized, being typically planar and layer-by-layer, respectively.

Whereas the formation of acoustic streaming around 2D sharp edges has been widely studied, acoustofluidic interactions around more complex 3D geometries have not been explored in a microfluidic environment. In this work, we examine the application of 3D sharp-edge microstructures to understand the effects of structure geometry on the direction and magnitude of 3D acoustic streaming fields. Here we fabricate and model structures with varying tip morphologies and characterize their influence on particle manipulation via ultrasonic streaming fields and acoustic radiation forces. We position these complex 3D microstructures in a substrate-based microchannel and acoustically actuate them via a coupled 7 MHz, bulk acoustic wave (BAW) transducer. These microstructures are fabricated utilizing two-photon polymerization, allowing for the creation of complex geometries with arbitrary configurations,

contoured surfaces, and precise tip angles, with the oscillation of these ~70 µm-high sub-wavelength microstructures producing 3D streaming vortices. To further examine the morphology of the 3D acoustic streaming produced, we employ numerical modeling to predict microstructure performance as a function of tip angle and experimentally validate these behaviors through particle image velocimetry. We demonstrate that unique streaming patterns result, including those that would not be feasible with conventional microfabrication strategies, where the size and orientation of fluid vortexes are determined by the 3D microstructure dimensions. In sum, the ability to generate high-magnitude, complex acoustic fields via 3D microstructures expands the range of platforms and applications for which sharp-edged effects can be utilized, flexibly allowing the number, scale, and magnitude of acoustic streaming vortices to be designed.

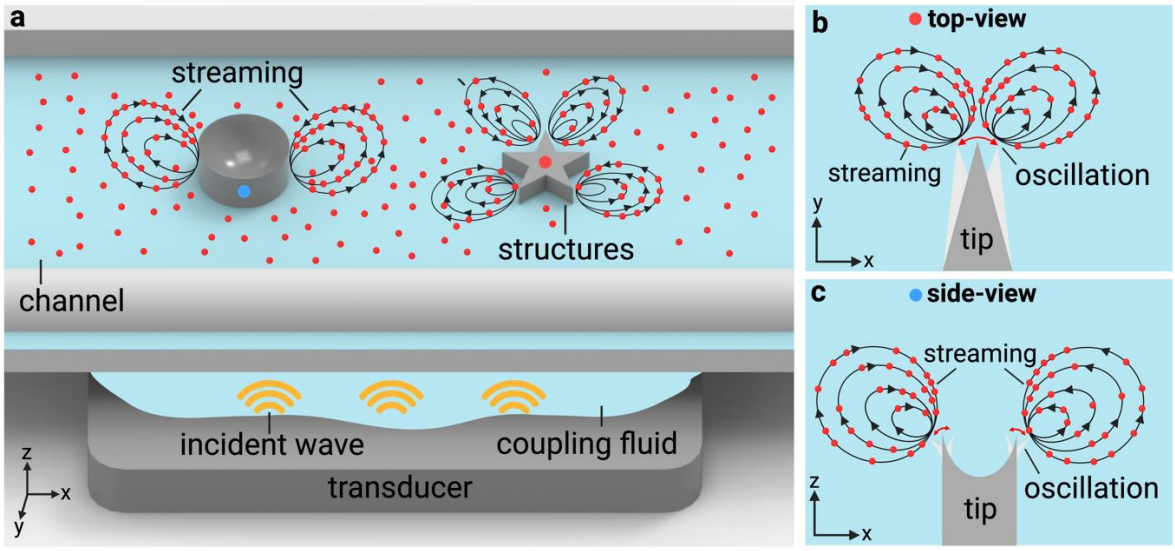

Fig. 1: Acoustic streaming of sharp-edge sub-wavelength 3D microstructures concept. (a) Acoustofluidic device schematic incorporating examples of 3D microstructures, where these are contained inside a microfluidic chamber bounded by a polydimethylsiloxane (PDMS) channel on glass. Piezoelectric actuation is coupled from the transducer to the microfluidic device via a thin water coupling layer. (b) Top view illustrating acoustic streaming caused by the oscillation of a microstructure sharp edge (e.g., the star in (a)). (c) Side-view illustrating acoustic streaming around a circular-shaped sharp edge formed by a pillar with a concave top surface.

2. Materials and methods

2.1 Concept and operating principles

Fig. 1 depicts the sharp-edge 3D microstructure device concept, where 3D structures are embedded inside a microfluidic PDMS chamber on fused silica. The fused silica chip is placed on a planar piezoelectric actuator ($LiNbO_3$). The top and bottom sides of the piezoelectric crystal are coated with conductive chromium/aluminum electrode layers. When the transducer is actuated with an alternating current (AC) electrical input, it generates a bulk-mode actuation along its thickness (z-axis), which couples to the silica substrate via a thin layer of water. The mechanical displacement of the silica layer induces coupled vibration in sharp-edge microstructures. Such a superstrate-based approach, where the microfluidic component is not directly bonded to the transducer, makes the microfluidic component interchangeable and

simplifies microchannel bonding. Particle manipulation effects in this acoustofluidic device are governed by the combined influences of acoustic radiation forces and acoustically induced steady flow, the latter termed acoustic streaming[50]. Acoustic streaming arises from the attenuation and transfer of acoustic energy into the bulk fluid flow, impacting particle motion through Stokes drag[51, 52].

Whereas both acoustic radiation forces and acoustic streaming are periodic and wavelength-scale in typical acoustofluidic systems, including those driven by bulk acoustic wave (BAW)[24] and surface acoustic wave (SAW)[52, 53] actuation, the use of sharp-edged microstructures here enables the generation of high streaming velocities and complex streaming vortices whose locations are determined by the local presence of these structures, rather than acoustic anti/nodal positions. Here acoustic streaming drives vortical motion around sharp tips, and the Gor'kov acoustic potential results in further particle motion in response to spatial variation in time-averaged acoustic fields, where this is calculated using a combination of the first-order pressure and velocity fields. As higher velocities result in lower potentials, and the highest first-order velocities are generated in the vicinity of sharp boundaries, the acoustic potential field gradient results in traction forces on polystyrene particles towards a microstructure's sharp-edges. The combination of acoustic streaming and acoustic radiation forces, with the former directing particles along fluid streamlines and the latter along acoustic force potential gradients[54], determine whether particles aggregate or are contained in vortices, with the interplay between these effects depending on particle size, driving frequency, and particle material properties[55].

2.2 Acoustic streaming at a sharp edge

The theory of acoustic streaming provides scaling laws for the streaming velocity around a wedge as a function of its sharp edge height a, and tip angle α[56]:

$$v_2 \sim \frac{\delta^{2n-1}}{a^{2n-2}}, \qquad n = \frac{\pi}{2\pi - \alpha}, \tag{1}$$

where $\delta = \sqrt{2\mu/\omega\rho_{0,w}} \approx 0.2$ μm is the viscous boundary layer thickness, μ is the fluid viscosity, ω is the angular frequency $\omega = 2\pi f$, $f = 7$ (MHz), $\rho_{0,w}$ is the fluid density, and where sharper tip angles result in higher streaming velocities at a given frequency. The estimation of the sharp interface height a is described in the Supplementary Note 1. This Equation is valid when the tip curvature radius ($r = 0.1$ μm in this study) is smaller than the viscous boundary layer thickness ($\delta = 0.2$ μm). Further, the utilized height (a) in this study ranges from 7 to 15 μm, which is substantially larger than the boundary layer thickness.

2.3 Computational analysis

In the numerical simulation we model a set of microstructures with tip angles ranging between 13°-146° in an axisymmetric study shown in Fig. S1. The microstructure dimensions are $h = 70$ μm and $w = 30$ μm, where micropillar edges were smoothed with a $r = 0.1$ μm fillet to represent the contouring that occurs during fabrication. The simulations were implemented with COMSOL Multiphysics 5.5 (COMSOL, Stockholm, Sweden) using the material parameters listed in Table S1 (see Supplementary Note 2).

2.4 Microstructure fabrication

Microstructures are designed using CAD software (Solid Edge 2021, Siemens) and prepared using DeScribe software (Nanoscribe, GmbH). The Photonic Professional GT2 (Nanoscribe, GmbH), a nanoscale 3D printing system utilizing two-photon polymerization, is employed for the fabrication of the polymeric microstructures. Here a femtosecond-pulsed laser with 100 fs pulse duration, 80 MHz repetition rate, and 780 nm wavelength is focused in an IP-Dip2 photoresist by an immersion objective lens (63x, NA = 0.8, WD = 200 μm) on a 0.5 mm thick fused silica substrate. Two-photon polymerization occurs at the focal point of the beam, which is scanned in three dimensions to build up a three-dimensional structure. The laser power is 25 mW, the beam scan speed is 100 mm s^{-1}, the vertical slicing distance is 0.1 μm, and the in-plane hatching distance is 0.1 μm. After laser writing, samples are developed in polyethylene glycol methyl ether acetate (50 mL) for 5 min to remove unexposed photoresist, followed by immersion in isopropyl alcohol (50 mL) for 5 min. Finally, the microstructures are gently blow-dried with N_2. Two shape types are explored in the examination of 3D acoustofluidic sharp-edged structures, with a sharp edge that is parametrically varied being either horizontal or vertical with respect to the transducer plane. This corresponds to the circle and star shape, respectively, in Fig. 1a, with cross sections of the respective sharp edges shown in Fig. 1b,c.

2.5 Experimental setup

The microfluidic device consists of a microfluidic channel bonded to a piece of fused silica, which is coupled by a thin layer of water to a piezoelectric transducer (see Fig. S2). The microfluidic cavity enclosing these microstructures is fabricated using a standard PDMS soft-lithography process (prepolymer to curing agent weight ratio at 10:1, Sylgard 184 Silicone Elastomer Kit, Dow corning Corp), in which the master mold for PDMS casting was fabricated with SU-8 (SU-8 3050, MicroChem, Newton, MA, USA) on a silicon wafer. The microfluidic cavity is a square 6 mm^2 with a height of 100 μm with a single inlet and outlet. The prefabricated microstructures on the fused silica substrate, together with the PDMS microchannel layer, are treated under air plasma (Plasma Etch, PE-50, NV, USA) to generate hydroxyl functional groups on the surfaces. The treated surfaces are then brought into contact and aligned to form a closed microfluidic channel. The piezoelectric transducer is actuated in thickness mode using sinusoidal signals from a function generator (Tektronix AFG3102C, Beaverton, USA) through an amplifier (Mini-Circuits TVA-R5-13A+, USA). Particle suspensions are injected into the microfluidic device via a syringe pump (Harvard Apparatus, MA, USA) at a flow rate of 25 μl/min, with flow stopped immediately prior to actuation, with the outlet being temporarily sealed to isolate the observation of particle motion in the absence of background flow. The observation was conducted using a fluorescence microscope (Olympus BX51, Japan) with a CCD camera (AmScope, CA, USA). We utilize green fluorescent polystyrene microspheres (Magsphere Inc., Pasadena, CA, USA) measuring 1 μm in diameter to visualize acoustic streaming vortices and particle manipulation. These particles are suspended in deionized water, containing 1% (w/v) Pluronic F127 (Sigma-Aldrich, USA) to prevent particle agglomeration and adhesion onto the microfluidic channel walls.

3. Results and discussion

3.1 Numerical modeling

Computational modeling can be used to explore the micromanipulation capabilities of acoustofluidic devices, potentially leading to performance optimization. In this work, we map the acoustic potential distribution and the steady streaming around sharp-edge microstructures to understand the impact of the tip angle dimensions on particle actuation. Sharp-edge microstructures are simulated in an axisymmetric (radially symmetric) study as shown in Fig. S3 within a simulated microfluidic environment. The bottom boundary has a prescribed uniform velocity actuation of 0.1 m/s which produces a pressure wave propagating upwards. Vertically actuated structures such as those shown here nevertheless exhibit complex oscillations, with vibrational motion in multiple orientations. Fig. S4 displays the sharp edge structure actuation mode, including displacement with a component orthogonal to the boundary vibration axis. The sharp tip experiences 3.8 times higher displacement magnitude than the bottom boundary of the structure, demonstrating an amplification effect. In Fig. 2a, the pressure amplitude within the fluid domain is plotted for a microstructure with a diameter of 30 μm and a height of 70 μm. This figure specifically highlights the acoustic field in the immediate vicinity of the microstructure. As the actuated microstructure is mechanically displaced, this produces a local pressure maxima on top of and inside the microstructure cavity. Fig. 2c displays the first-order fluid velocity magnitude, showing that peak values are located at the oscillating sharp-edge boundary.

Modelling of particle motion in the vicinity of sharp-tips takes into account the acoustic radiation forces and acoustic streaming. The acoustophoretic force is primarily governed by the Gor'kov potential U^{rad}, which is a function of both pressure and velocity fields. Particles in the fluid domain are directed toward regions of minimum acoustic potential. The potential U^{rad} is the sum of the monopole U_{mp}^{rad} and dipole U_{dp}^{rad} terms, which depend on the local time-averaged complex-valued pressure $\langle p_1^2 \rangle$ and velocity $\langle \boldsymbol{v}_1^2 \rangle$ fields, respectively, as detailed in Eq. (S22). Whereas the pressure and velocity distribution are intrinsic to the fluidic domain in the vicinity of a structure, the potential distribution is a function of a particle's interaction with these fields, where the results in Fig. 2b,d are plotted for a representative 1 μm polystyrene particle. The monopole term distribution in Fig. 2b is determined by the pressure amplitude and thus reaches its local maxima inside the microstructure cavity, with local minima at the top and bottom boundaries of the domain. The dipole term in Fig. 2d, in turn, reaches its minimum near the sharp edges at the top of the microstructure, coinciding with the locations of the highest acoustic velocity. As the dipole component is of substantially greater magnitude than that of the monopole one, the resulting Gor'kov potential U^{rad} in Fig. 2f has a minimum near the sharp-edge boundary of microstructures and dissipates rapidly outside of this region, where Fig. 2f plots U^{rad} across the axisymmetric cross sections of microstructures with tip angles ranging from 13°-146°.

Additionally, the steady streaming flow $\boldsymbol{v_2}$, arising from viscous dissipation, exerts fluid drag forces on suspended particles as described by Eq. (S23). Fig. 2g shows the acoustic streaming velocity magnitudes around microstructures overlayed with their corresponding flow streamlines. In the case of a conventional 2D oscillating wedge, fluid outflow occurs along the centerline of a sharp edge, accompanied by inflow from the sides, producing two symmetric vortices[56]. Uniquely for our case, our structure induces a double toroidal vortex in the vicinity of a sharp tip ($\alpha = 13°$), and a single toroidal vortex in the tip vicinity at larger angles. Fig. 2e plots the maximum acoustic streaming velocity as a function of the edge angle and illustrates that sharper-angled microstructures produce higher streaming velocities. This observed dependence generally aligns with the analytical relation, Eq. (1), which denotes the streaming velocity around a side-moving wedge (see Fig. 2e), though non-zero streaming

velocities at higher tip angles in the simulation case may arise due to contributions from acoustofluidic-structure interactions besides those at the tip region.

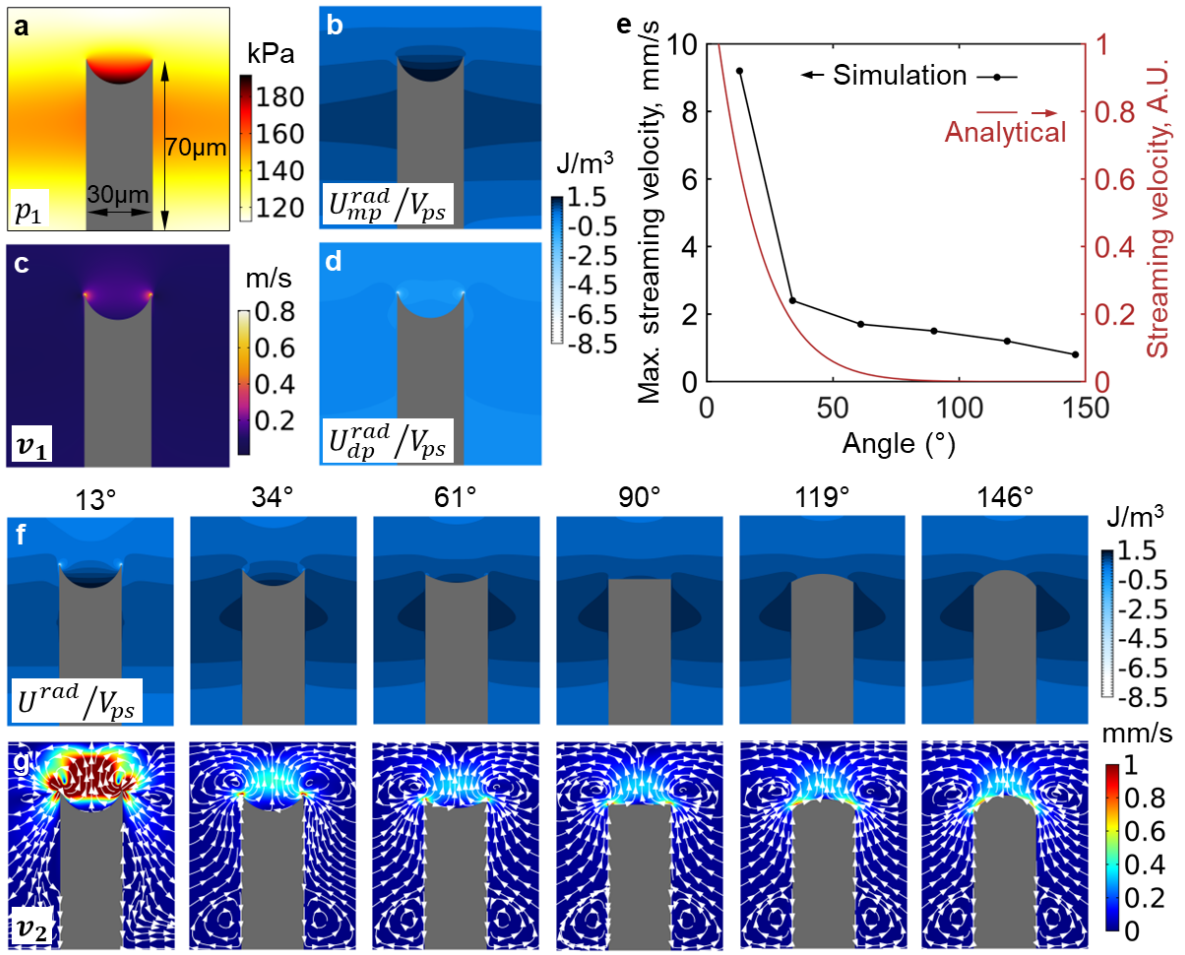

Fig. 2. Numerical modeling results for the axisymmetric structure with $w = 30\ \mu m, h = 70\ \mu m$ actuated at 7 MHz. (a) Pressure amplitude, with local pressure maxima inside the microstructure cavity. (b) The normalized Gor'kov potential monopole (pressure dependent) component. (c) High first-order fluid velocity amplitude near the sharp edges of the oscillating structure. (d) The dipole (velocity-dependent) component of the potential. (e) Maximum streaming velocity as a function of the sharp-edge angle (computational) and analytical streaming velocity scaling law (Eq. 1). (f) The combined Gor'kov potential with minima near the sharp edges of microstructures with sharper angles. (g) Acoustic streaming velocity magnitude of microstructures overlayed with flow streamlines.

3.2 Parallel microstructure streaming

There are two orientations for sharp edges that are experimentally examined in this work, namely where the sharp edge that is varied is in the plane of the transducer (parallel) and where it is orthogonal to it. In the first case, we examine a circular pillar in line with that depicted in Fig. 2 in which the edge angle of the top surface is varied, transitioning from a concave to a convex shape at its top with increasing tip angle. The ultrasonic microstreaming fields around individual 3D microstructures are first analyzed by arranging three sets of each of the 6 corresponding angled sharp-edged structures. A total of 18 structures for each analysis are thus positioned into an evenly spaced array with 500 μm between neighboring structures to allow sufficient space to observe particle streaming trajectories. A frequency of 7 MHz is applied to the transducer used in this microfluidic setup, similar to that used in previous work examining oscillating microstructures[60]. This same frequency is further observed to provide the strongest acoustic response for microstructures of this size and thickness of superstrate and is in good agreement with the simulation results, as well as with other work utilizing this thickness and crystallographic cut of $LiNbO_3$[61]. While higher frequencies may be desirable from the perspective of maximizing energy deposition in fluids, their application may result in excessive wave dissipation leading to undesirable vortices throughout the fluid that are not localized around sharp tips, with the acoustic attenuation (and therefore acoustic body forces in the fluid) scaling with the square of the applied frequency. As forecasted by our numerical modeling results, experiments demonstrate that suspended microparticles migrate towards areas of acoustic potential minima located at the sharp-edge apex. The 1 μm microparticles are further trapped inside the acoustic streaming vortices and exhibit particle trajectories that correspond to the simulation results. Fig. 3a shows to-scale cross-sections of the corresponding CAD model, whereby the volume of each structure is matched by altering the height to ensure the acoustophoretic response is primarily dictated by the microstructure angle and not the mass difference between pillars. Fig. 3b displays helium ion microscopy images of each structure to illustrate the smooth curvature at the top of each pillar and the accuracy of the fabrication procedure, with ~100 nm resolution dimensions at the sharp-edge interface.

Fig. 3c shows the acoustic streaming flow fields observed for each sharp-edge structure, where the red arrows delineate the particle streaming direction. Notably, structures with smaller edge angles exhibit the highest acoustic streaming velocities, with the spatial extent of their 3D vortices extending beyond a radius of ~300 μm from the center of the structure (for the 13° case) representing streaming fields that extend ~20x the microstructure diameter. Micropillars with 13°, 34°, and 90° tip angles exhibit particle attraction occurring along the edge boundary where their dynamics are governed by the interplay of acoustophoretic and streaming-induced forces. In the 90° case, for example, microparticles are initially attracted to the acoustic potential minima at the sharp edge interface and remain trapped while rotating around the circular edge. As it is intrinsically difficult to capture 3D acoustic streaming fields in single 2D images, Supplementary Movie 1 further displays these behaviors. Particle tracking and velocity mapping are realized by implementing particle image velocimetry, where Fig. 3d plots the average velocity magnitude in (μm/s) as a function of the structure's apex angle. This result further evidences an agreement in the trend of the numerical simulation result shown in Fig. 2e and Fig. 3d, where the velocity magnitude decreases as the tip angle increases. To visualize the acoustic streaming fields and regions of high velocities surrounding microstructures, Fig. 3e shows an absolute velocity magnitude map in (μm/s).

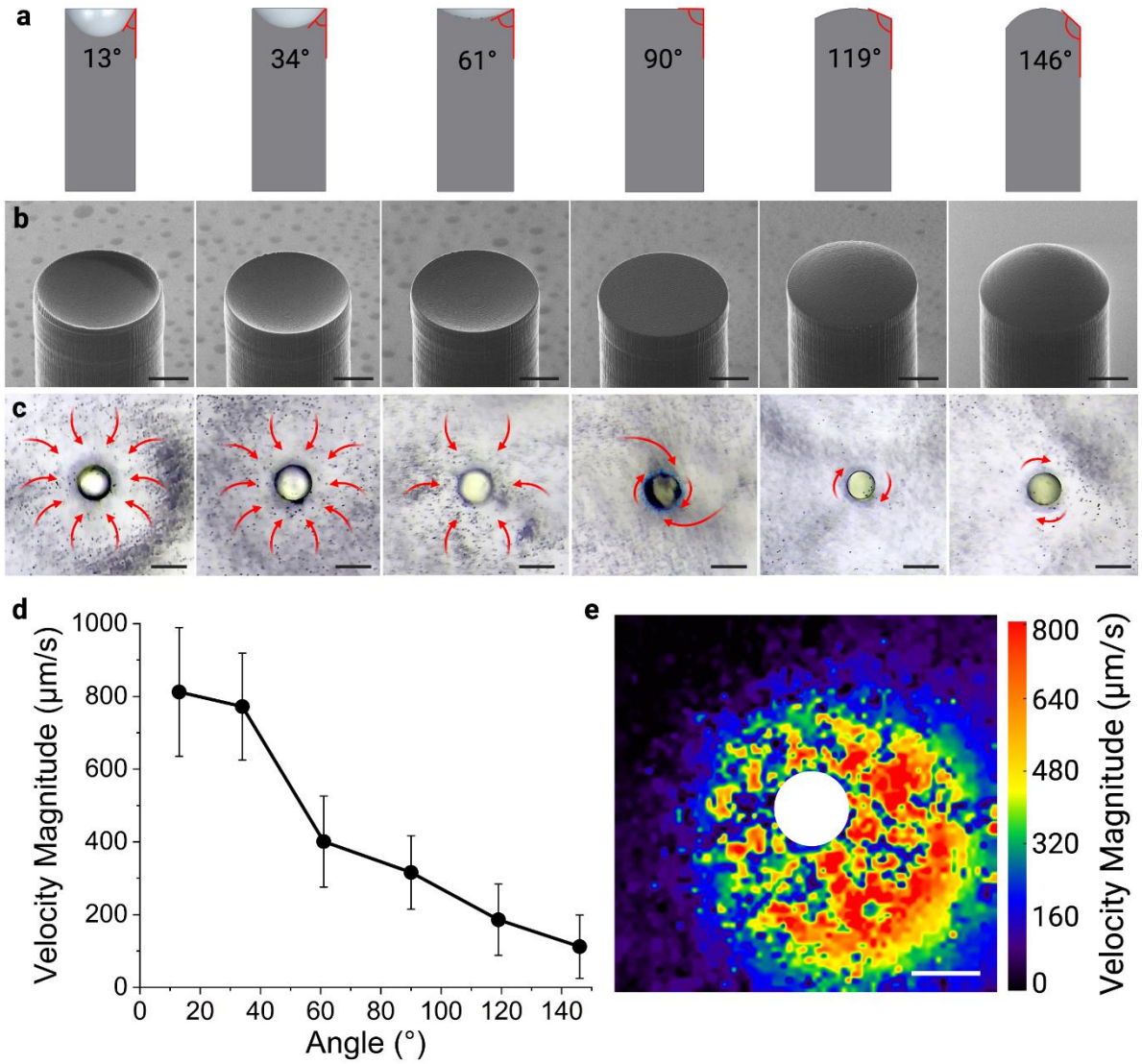

Fig. 3. Acoustic streaming analysis of 3D microstructures. (a) Cross-section of microstructure models with varying sharp-edge angles. (b) Helium ion microscopy (HIM) images of 3D microstructures. Scale bars are 10 µm (c) Optical brightfield images capturing movement and aggregation behaviors of 1 µm particles, red arrows indicate particle trajectory direction, blue area indicates regions of particle aggregation. Scale bars are 30 µm. (d) Average particle velocity magnitude with varying sharp-edge angle microstructures, where error bars are ±one standard deviation. (e) Absolute velocity magnitude map around the 13° microstructure. Scale bar is 30 µm.

3.3 Orthogonal microstructure streaming

Alternatively, the sharp edges of microstructures can be orthogonal to the transducer plane. To assess the ultrasonic streaming fields of such sharp-edged microstructures, a 5-point star geometry was chosen, as it allows structures to have a wide range of tip angles in which streaming fields and particle manipulation can be observed. These are placed in the same arrangement as previously to allow sufficient space to observe particle streaming trajectories without interference from neighboring structures, and similarly actuated at a 7 MHz frequency. Fig. 4a shows a top-view of the corresponding CAD model to illustrate how the sharp-edge tips are designed, whereby the volume (and thus mass) of each structure is matched to ensure

the acoustophoretic response is primarily dictated by the microstructures angle. To account for this, microstructures with tip morphologies ranging from 15° to 108° were fabricated with off-resonance heights from 75 µm to 45 µm, respectively. Fig. 4b displays helium ion microscopy images of each structure. Fig. 4c shows the acoustic streaming flow fields for each angle and red arrows delineate the particle streaming direction. Microstructures with 15°-51° tip angles exhibit large vortices focused on the sharp edges of each star tip, with particle aggregation within these vortices. Angles at or below 51° exhibit the greatest observable acoustic streaming velocities, with more clearly defined vortexes coincident with sharp tips. Microstructures with tip angles ranging from 87°-108° demonstrate a further change in the streaming field locations and a reduction in the spatial extent of the resulting vortices compared to sharper tip angles, and can be further visualized in Supplementary Movie 2. Particle tracking is realized by implementing particle image velocimetry, where Fig. 4d plots the average velocity magnitude in (µm/s) as a function of the structure's apex angle and highlights that as the tip angle increases, the velocity magnitude significantly decreases. Fig. 4e displays a representative velocity magnitude map of the 36° structure which highlights the appearance of high streaming magnitudes across the vortex extents.

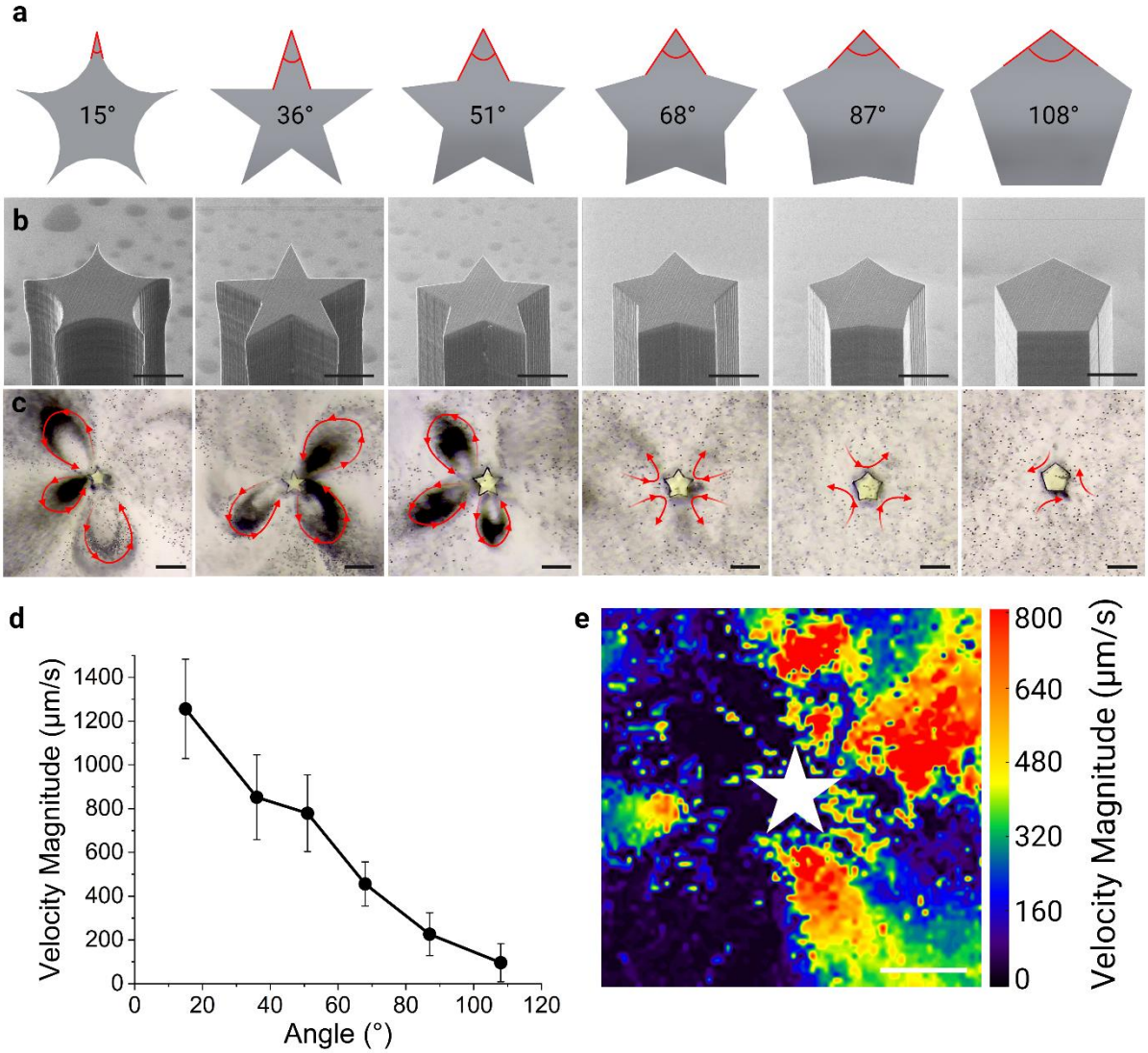

Fig. 4. Acoustic streaming analysis of planar microstructures. (a) Top-view of CAD microstructure models with varying sharp-edge angles. (b) Helium ion microscopy (HIM) images of planar microstructures. Scale bars are 10 µm (c) Optical brightfield images capturing movement and aggregation behaviors of 1 µm particles, red arrows indicate particle trajectory

direction. Scale bars are 30 μm. (d) Average velocity magnitude of microparticles with varying sharp-edge angles, error bars are standard deviation. (e) Absolute velocity magnitude map of the 36° microstructure. Scale bar is 30 μm.

4. Discussion and conclusions

Whereas prior work with oscillating bubbles and structures primarily evidenced dipole or quadrupole streaming[62, 63], in line with the resonance behavior of these elements, defining 3D microstructures with arbitrary geometries readily permits the formation of streaming with even odd numbers of vortices in different orientations. Here, for instance, utilizing a single continuous sharp edge at the top of a micropillar, a single streaming vortex with a rotational axis parallel to the transducer plane is formed. On the other hand, when employing orthogonally oriented shapes, such as the star-shaped microstructures in this study, we observe the formation of strong vortexes with streaming magnitudes dependent on the tip angles. The number of vortices, the strength and the extent of each vortex may not be uniform, however, due to the presence of additional vibrational modes and slight variations in cross-sectional amplitude. These factors can lead to preferential directional particle migration, as observed elsewhere [54]. Further, while off target vibrational modes in micropillars may result from small variations in vibration amplitude and non-symmetric geometries in fabricated microstructures, the simulation modeling performed using a unidirectional vibration amplitude boundary condition nevertheless replicates the primary streaming features observed experimentally, with, for instance, a toroidal vortex coincident with the sharp tip ring in Fig. 2 and Fig. 3.

Together these results demonstrate the additional flexibility afforded by utilizing sharp edges on 3D microstructures compared to those arising from planar fabrication approaches, where the orientation and direction of streaming vortexes can be determined using appropriate structural elements. Further, these acoustic fields, arising from evanescent effects in sub-wavelength features where the submicron tip dimensions are orders of magnitude smaller than the acoustic wavelength, are nevertheless capable of generating acoustic streaming vortexes have extents even larger than the acoustic wavelength. The location of these vortexes is further determined by the location of sharp edge elements, rather than the position of nodal/antinodal positions in a standing wave field. This compares to previous work examining standing wave streaming in which streaming vortexes are periodic and extend half-fluid wavelengths on either side of nodal positions[64]. This work therefore demonstrates the potential for microstructure geometries to produce tailored streaming fields, where this may extend beyond the symmetric geometries shown here to those including anti-symmetric designs, and with variations in the orientation and angle of sharp tips. Future work may focus on 3D simulations and testing such devices in which the direction, magnitude and extent of streaming is an important factor.

A further finding of this work is the critical importance of tip angle in 3D microstructures. This is enabled by the examination of acoustic streaming fields in parametrically altered tip morphologies on sharp-edge microstructures, with higher streaming velocities resulting from sharper angles. While this is corroborated by previous results examining sharp-edges[28, 32, 47], there utilizing 2-dimensional single edges produced via silicon etching, our present work represents the first such examination of this effect around 3D microfabricated elements. The fabrication of these 3D microstructures is enabled by the first implementation of two-photon lithography for this purpose, generating precise submicron tip length scales and smooth surfaces. Compared to acoustic approaches that rely on the planar architectures, we

demonstrate the potential of arbitrarily designed 3D microstructures to alter the direction and behavior of 3D streaming vortices as a function of the geometry shape and the orientation of oscillating sharp edges, with both in-plane and out-of-plane vortex orientations. We have numerically modeled and experimental demonstrated this by altering the tip angle and geometric configuration of the microstructures, with edges that have various orientations and shapes.

Having demonstrated the acoustic streaming-based manipulation of microparticles, this work exhibits the potential for complex manipulation of particles of varying sizes and characteristics, where the number, shape and orientation of acoustic streaming vortices can be controlled, facilitating applications in bioparticle, cell, and microorganism studies. Precise control within microfluidic environments containing 3D microstructures can be effectively harnessed for a multitude of lab-on-chip applications, encompassing tasks such as cell lysis, phenotyping, and volumetric imaging[65, 66]. While the application of acoustic streaming via 3D microstructures is accordingly undeveloped, where we demonstrate examine this approach here for the first time, this approach offers the potential to amplify and arbitrarily orient fluid vortices and shear forces to improve a range of applications where these are utilized, including on-demand cell lysis, rapid mixing and bioparticle manipulation applications. In the latter case, 3D structural elements provide increased surface areas for sample interactions and enables the design of trapping locations through tailorable streaming fields. Complex 3D architectures also hold potential for advances in multiplexed capture of different bioparticles simultaneously, enabling parallel processing and high-throughput screening in applications like drug discovery and molecular diagnostics. Rotational manipulation for 3D image reconstruction has the potential to be improved as well, where the ability to orient rotation in different axes can improve imaging fidelity [67]. In sum, this approach highlights the versatility of microprinted 3D geometries to produce defined acoustic and streaming fields, expanding the range of micromanipulation applications for which sharp-edge geometries can be utilized.

Conflicts of interest

The authors declare that they have no known competing financial interests or personal relationships that could have appeared to influence the work reported in this paper.

Acknowledgements

This work was performed in part at the Melbourne Centre for Nanofabrication (MCN), RMIT Micro Nano Research Facility (MNRF), Materials Characterisation and Fabrication Platform (MCFP) at the University of Melbourne and the Victorian Node of the Australian National Fabrication Facility (ANFF). Dr. Collins is the recipient of a Discovery Early Career Researcher Award from the Australian Research Council (DECRA, DE200100909), and funding from the National Health and Medical Research Council (Ideas, APP2003446). Select figures were created with BioRender.com

References

[1] E.K. Sackmann, A.L. Fulton, D.J. Beebe, The present and future role of microfluidics in biomedical research, Nature 507(7491) (2014) 181-9.
[2] A. Reece, B. Xia, Z. Jiang, B. Noren, R. McBride, J. Oakey, Microfluidic techniques for high throughput single cell analysis, Curr Opin Biotechnol 40 (2016) 90-96.
[3] P.S. Dittrich, A. Manz, Lab-on-a-chip: microfluidics in drug discovery, Nature Reviews Drug Discovery 5(3) (2006) 210-218.

[4] E.K. Sackmann, A.L. Fulton, D.J. Beebe, The present and future role of microfluidics in biomedical research, Nature 507(7491) (2014) 181-189.
[5] Q. Zhong, H. Ding, B. Gao, Z. He, Z. Gu, Advances of Microfluidics in Biomedical Engineering, Advanced Materials Technologies 4(6) (2019) 1800663.
[6] B. Zhang, A. Korolj, B.F.L. Lai, M. Radisic, Advances in organ-on-a-chip engineering, Nature Reviews Materials 3(8) (2018) 257-278.
[7] X. Wang, S. Chen, M. Kong, Z. Wang, K.D. Costa, R.A. Li, D. Sun, Enhanced cell sorting and manipulation with combined optical tweezer and microfluidic chip technologies, Lab on a Chip 11(21) (2011) 3656-3662.
[8] H. Zhang, K.-K. Liu, Optical tweezers for single cells, Journal of the Royal Society interface 5(24) (2008) 671-690.
[9] H. Yun, K. Kim, W.G. Lee, Cell manipulation in microfluidics, Biofabrication 5(2) (2013) 022001.
[10] Y. Pan, X. Du, F. Zhao, B. Xu, Magnetic nanoparticles for the manipulation of proteins and cells, Chemical Society Reviews 41(7) (2012) 2912-2942.
[11] H. Shafiee, J.L. Caldwell, M.B. Sano, R.V. Davalos, Contactless dielectrophoresis: a new technique for cell manipulation, Biomedical microdevices 11 (2009) 997-1006.
[12] Z.R. Gagnon, Cellular dielectrophoresis: Applications to the characterization, manipulation, separation and patterning of cells, Electrophoresis 32(18) (2011) 2466-2487.
[13] K. Kolesnik, P. Segeritz, D.J. Scott, V. Rajagopal, D.J. Collins, Sub-wavelength acoustic stencil for tailored micropatterning, Lab Chip (2023).
[14] A. Fakhfouri, C. Devendran, A. Ahmed, J. Soria, A. Neild, The size dependant behaviour of particles driven by a travelling surface acoustic wave (TSAW), Lab Chip 18(24) (2018) 3926-3938.
[15] T. Henighan, A. Chen, G. Vieira, A.J. Hauser, F.Y. Yang, J.J. Chalmers, R. Sooryakumar, Manipulation of Magnetically Labeled and Unlabeled Cells with Mobile Magnetic Traps, Biophysical Journal 98(3) (2010) 412-417.
[16] A. Blázquez-Castro, Optical Tweezers: Phototoxicity and Thermal Stress in Cells and Biomolecules, Micromachines 10(8) (2019) 507.
[17] N. Abd Rahman, F. Ibrahim, B. Yafouz, Dielectrophoresis for Biomedical Sciences Applications: A Review, Sensors 17(3) (2017) 449.
[18] Z. Chen, X. Liu, M. Kojima, Q. Huang, T. Arai, Advances in Micromanipulation Actuated by Vibration-Induced Acoustic Waves and Streaming Flow, Applied Sciences 10(4) (2020) 1260.
[19] J. Rufo, F. Cai, J. Friend, M. Wiklund, T.J. Huang, Acoustofluidics for biomedical applications, Nature Reviews Methods Primers 2(1) (2022).
[20] D.J. Collins, R. O'Rorke, A. Neild, J. Han, Y. Ai, Acoustic fields and microfluidic patterning around embedded micro-structures subject to surface acoustic waves, Soft Matter 15(43) (2019) 8691-8705.
[21] S. Mohanty, I.S.M. Khalil, S. Misra, Contactless acoustic micro/nano manipulation: a paradigm for next generation applications in life sciences, Proc Math Phys Eng Sci 476(2243) (2020) 20200621.
[22] M. Wu, A. Ozcelik, J. Rufo, Z. Wang, R. Fang, T. Jun Huang, Acoustofluidic separation of cells and particles, Microsyst Nanoeng 5 (2019) 32.
[23] G.T. Silva, J.H. Lopes, J.P. Leão-Neto, M.K. Nichols, B.W. Drinkwater, Particle Patterning by Ultrasonic Standing Waves in a Rectangular Cavity, Physical Review Applied 11(5) (2019).
[24] C. Bouyer, P. Chen, S. Guven, T.T. Demirtas, T.J. Nieland, F. Padilla, U. Demirci, A Bio-Acoustic Levitational (BAL) Assembly Method for Engineering of Multilayered, 3D Brain-

Like Constructs, Using Human Embryonic Stem Cell Derived Neuro-Progenitors, Adv Mater 28(1) (2016) 161-7.
[25] K. Kolesnik, M. Xu, P.V.S. Lee, V. Rajagopal, D.J. Collins, Unconventional acoustic approaches for localized and designed micromanipulation, Lab Chip 21(15) (2021) 2837-2856.
[26] M. Xu, W.S. Harley, Z. Ma, P.V.S. Lee, D.J. Collins, Sound-speed Modifying Acoustic Metasurfaces for Acoustic Holography, Advanced Materials (2023) 2208002.
[27] Z. Ma, A.W. Holle, K. Melde, T. Qiu, K. Poeppel, V.M. Kadiri, P. Fischer, Acoustic Holographic Cell Patterning in a Biocompatible Hydrogel, Adv Mater 32(4) (2020) e1904181.
[28] C. Zhang, X. Guo, P. Brunet, M. Costalonga, L. Royon, Acoustic streaming near a sharp structure and its mixing performance characterization, Microfluidics and Nanofluidics 23(9) (2019).
[29] R. Rasouli, M. Tabrizian, Rapid Formation of Multicellular Spheroids in Boundary-Driven Acoustic Microstreams, Small 17(39) (2021) e2101931.
[30] B. Liu, M. Qiao, S. Zhang, J. Yang, A Bi-Directional Acoustic Micropump Driven by Oscillating Sharp-Edge Structures, Micromachines 14(4) (2023) 860.
[31] J. Durrer, P. Agrawal, A. Ozgul, S.C.F. Neuhauss, N. Nama, D. Ahmed, A robot-assisted acoustofluidic end effector, Nat Commun 13(1) (2022) 6370.
[32] C. Zhang, X. Guo, L. Royon, P. Brunet, Unveiling of the mechanisms of acoustic streaming induced by sharp edges, Physical Review E 102(4) (2020).
[33] P.-H. Huang, C.Y. Chan, P. Li, Y. Wang, N. Nama, H. Bachman, T.J. Huang, A sharp-edge-based acoustofluidic chemical signal generator, Lab on a Chip 18(10) (2018) 1411-1421.
[34] W. Connacher, N. Zhang, A. Huang, J. Mei, S. Zhang, T. Gopesh, J. Friend, Micro/nano acoustofluidics: materials, phenomena, design, devices, and applications, Lab on a Chip 18(14) (2018) 1952-1996.
[35] Z. Chen, P. Liu, X. Zhao, L. Huang, Y. Xiao, Y. Zhang, J. Zhang, N. Hao, Sharp-edge acoustic microfluidics: Principles, structures, and applications, Applied Materials Today 25 (2021).
[36] N. Nama, P.-H. Huang, T.J. Huang, F. Costanzo, Investigation of acoustic streaming patterns around oscillating sharp edges, Lab Chip 14(15) (2014) 2824-2836.
[37] P.B. Muller, H. Bruus, Numerical study of thermoviscous effects in ultrasound-induced acoustic streaming in microchannels, Phys Rev E Stat Nonlin Soft Matter Phys 90(4) (2014) 043016.
[38] P.B. Muller, R. Barnkob, M.J.H. Jensen, H. Bruus, A numerical study of microparticle acoustophoresis driven by acoustic radiation forces and streaming-induced drag forces, Lab on a Chip 12(22) (2012) 4617-4627.
[39] M.B. Dentry, L.Y. Yeo, J.R. Friend, Frequency effects on the scale and behavior of acoustic streaming, Phys Rev E Stat Nonlin Soft Matter Phys 89(1) (2014) 013203.
[40] J. Lei, P. Glynne-Jones, M. Hill, Comparing methods for the modelling of boundary-driven streaming in acoustofluidic devices, Microfluidics and Nanofluidics 21(2) (2017).
[41] P.-H. Huang, Y. Xie, D. Ahmed, J. Rufo, N. Nama, Y. Chen, C.Y. Chan, T.J. Huang, An acoustofluidic micromixer based on oscillating sidewall sharp-edges, Lab on a Chip 13(19) (2013) 3847.
[42] A. Pavlic, C.L. Harshbarger, L. Rosenthaler, J.G. Snedeker, J. Dual, Sharp-edge-based acoustofluidic chip capable of programmable pumping, mixing, cell focusing, and trapping, Physics of Fluids 35(2) (2023) 022006.
[43] Z. Wang, P.H. Huang, C. Chen, H. Bachman, S. Zhao, S. Yang, T.J. Huang, Cell lysis via acoustically oscillating sharp edges, Lab Chip 19(24) (2019) 4021-4032.
[44] L. Feng, B. Song, Y. Chen, S. Liang, Y. Dai, Q. Zhou, D. Chen, X. Bai, Y. Feng, Y. Jiang, D. Zhang, F. Arai, On-chip rotational manipulation of microbeads and oocytes using acoustic

microstreaming generated by oscillating asymmetrical microstructures, Biomicrofluidics 13(6) (2019) 064103.
[45] B. Kang, J. Shin, H.J. Park, C. Rhyou, D. Kang, S.J. Lee, Y.S. Yoon, S.W. Cho, H. Lee, High-resolution acoustophoretic 3D cell patterning to construct functional collateral cylindroids for ischemia therapy, Nat Commun 9(1) (2018) 5402.
[46] Z. Ma, Y. Zhou, F. Cai, L. Meng, H. Zheng, Y. Ai, Ultrasonic microstreaming for complex-trajectory transport and rotation of single particles and cells, Lab Chip 20(16) (2020) 2947-2953.
[47] A.A. Doinikov, M.S. Gerlt, A. Pavlic, J. Dual, Acoustic streaming produced by sharp-edge structures in microfluidic devices, Microfluidics and Nanofluidics 24(5) (2020).
[48] C. Zhang, X. Guo, L. Royon, P. Brunet, Acoustic Streaming Generated by Sharp Edges: The Coupled Influences of Liquid Viscosity and Acoustic Frequency, Micromachines 11(6) (2020) 607.
[49] Z. Ghorbani Kharaji, V. Kalantar, M. Bayareh, Acoustic sharp-edge-based micromixer: a numerical study, Chemical Papers 76(3) (2022) 1721-1738.
[50] M. Settnes, H. Bruus, Forces acting on a small particle in an acoustical field in a viscous fluid, Phys Rev E Stat Nonlin Soft Matter Phys 85(1 Pt 2) (2012) 016327.
[51] M. Wiklund, R. Green, M. Ohlin, Acoustofluidics 14: Applications of acoustic streaming in microfluidic devices, Lab Chip 12(14) (2012) 2438-51.
[52] C. Devendran, D.J. Collins, A. Neild, The role of channel height and actuation method on particle manipulation in surface acoustic wave (SAW)-driven microfluidic devices, Microfluidics and Nanofluidics 26(2) (2022).
[53] Z. Tian, Z. Wang, P. Zhang, T.D. Naquin, J. Mai, Y. Wu, S. Yang, Y. Gu, H. Bachman, Y. Liang, Z. Yu, T.J. Huang, Generating multifunctional acoustic tweezers in Petri dishes for contactless, precise manipulation of bioparticles, Science Advances 6(37) (2020) eabb0494.
[54] D.J. Collins, Z. Ma, Y. Ai, Highly Localized Acoustic Streaming and Size-Selective Submicrometer Particle Concentration Using High Frequency Microscale Focused Acoustic Fields, Anal Chem 88(10) (2016) 5513-22.
[55] A.A. Doinikov, M.S. Gerlt, J. Dual, Acoustic Radiation Forces Produced by Sharp-Edge Structures in Microfluidic Systems, Physical Review Letters 124(15) (2020).
[56] M. Ovchinnikov, J. Zhou, S. Yalamanchili, Acoustic streaming of a sharp edge, The Journal of the Acoustical Society of America 136(1) (2014) 22-29.
[57] P. Hahn, O. Schwab, J. Dual, Modeling and optimization of acoustofluidic micro-devices, Lab on a Chip 14(20) (2014) 3937-3948.
[58] J.S. Bach, H. Bruus, Theory of pressure acoustics with viscous boundary layers and streaming in curved elastic cavities, The Journal of the Acoustical Society of America 144(2) (2018) 766-784.
[59] L.P. Gor'kov, On the forces acting on a small particle in an acoustical field in an ideal fluid, Sov. Phys. Dokl., 1962, pp. 773-775.
[60] W.S. Harley, K. Kolesnik, M. Xu, D.E. Heath, D.J. Collins, 3D Acoustofluidics via Sub-Wavelength Micro-Resonators, Advanced Functional Materials (2022).
[61] S. Collignon, O. Manor, J. Friend, Improving and Predicting Fluid Atomization via Hysteresis-Free Thickness Vibration of Lithium Niobate, Advanced Functional Materials 28(8) (2018) 1704359.
[62] J. Wu, G. Du, Streaming generated by a bubble in an ultrasound field, The Journal of the Acoustical Society of America 101(4) (1997) 1899-1907.
[63] P. Tho, R. Manasseh, A. Ooi, Cavitation microstreaming patterns in single and multiple bubble systems, Journal of Fluid Mechanics 576 (2007) 191-233.

[64] P.B. Muller, R. Barnkob, M.J.H. Jensen, H. Bruus, A numerical study of microparticle acoustophoresis driven by acoustic radiation forces and streaming-induced drag forces, Lab on a Chip 12(22) (2012) 4617.
[65] I. Leibacher, P. Hahn, J. Dual, Acoustophoretic cell and particle trapping on microfluidic sharp edges, Microfluidics and Nanofluidics 19(4) (2015) 923-933.
[66] A. Ozcelik, N. Nama, P.H. Huang, M. Kaynak, M.R. McReynolds, W. Hanna-Rose, T.J. Huang, Acoustofluidic Rotational Manipulation of Cells and Organisms Using Oscillating Solid Structures, Small 12(37) (2016) 5120-5125.
[67] T. Tang, Y. Hosokawa, T. Hayakawa, Y. Tanaka, W. Li, M. Li, Y. Yalikun . Rotation of biological cells: fundamentals and applications. Engineering. 1(10) (2022) 110-26.